LETTER

doi:10.1038/nature25011

Photonic topological boundary pumping as a probe of 4D quantum Hall physics

Oded Zilberberg[1], Sheng Huang[2], Jonathan Guglielmon[3], Mohan Wang[2], Kevin P. Chen[2], Yaacov E. Kraus[4]‡ & Mikael C. Rechtsman[3]

When a two-dimensional (2D) electron gas is placed in a perpendicular magnetic field, its in-plane transverse conductance becomes quantized; this is known as the quantum Hall effect[1]. It arises from the non-trivial topology of the electronic band structure of the system, where an integer topological invariant (the first Chern number) leads to quantized Hall conductance. It has been shown theoretically that the quantum Hall effect can be generalized to four spatial dimensions[2–4], but so far this has not been realized experimentally because experimental systems are limited to three spatial dimensions. Here we use tunable 2D arrays of photonic waveguides to realize a dynamically generated four-dimensional (4D) quantum Hall system experimentally. The inter-waveguide separation in the array is constructed in such a way that the propagation of light through the device samples over momenta in two additional synthetic dimensions, thus realizing a 2D topological pump[5–8]. As a result, the band structure has 4D topological invariants (known as second Chern numbers) that support a quantized bulk Hall response with 4D symmetry[7]. In a finite-sized system, the 4D topological bulk response is carried by localized edge modes that cross the sample when the synthetic momenta are modulated. We observe this crossing directly through photon pumping of our system from edge to edge and corner to corner. These crossings are equivalent to charge pumping across a 4D system from one three-dimensional hypersurface to the spatially opposite one and from one 2D hyperedge to another. Our results provide a platform for the study of higher-dimensional topological physics.

Topology manifests naturally in solid-state systems. In insulators, electrons fill electronic states below the bandgap of the system. These states can be mapped mathematically onto abstract shapes that are characterized by a topological invariant. The realization that these topological invariants manifest as quantized bulk responses, and through corresponding topologically protected boundary states, has revolutionized our understanding of material properties. These phenomena have been explored in several fields in systems beyond solid-state materials, including photonic[6,8–13] and ultracold atomic[14–17] systems.

The introduction of topology into photonics[9] has opened up many avenues of research. Much of this research has focused on the experimental observation of topologically protected edge states in systems such as photonic crystals in the microwave domain[10,13], as well as arrays of waveguides[6,8,11] and integrated ring resonators at optical frequencies[12]. In these systems, dielectric structures act as lattices for light, leading to topological 2D photonic bands. Beyond two dimensions, experiments with three-dimensional (3D) lattices have unveiled topological features[18] such as Weyl points[19,20].

The study of topological phases can be defined and understood mathematically beyond three dimensions, with a hallmark example being the 4D quantum Hall effect[2–4,7]. In 2D quantum Hall systems, energy bands are characterized by the first Chern number, which quantizes the Hall conductance and therefore counts one-dimensional (1D) chiral edge states in the system. In 4D systems, energy bands are characterized by another topological invariant—the second Chern number[2–4,7,21–24]. Similarly to the 2D case, the 4D invariant manifests through an additional quantized bulk response with 4D hypersurface phenomena. Until recently, the latter seemed only of theoretical interest because its realization requires four spatial dimensions. The flexibility of atomic and photonic systems, however, has inspired proposals to include synthetic dimensions to realize higher-dimensional topological physics[25–28].

The concept of topological pumps lends itself well to synthetic dimensions and higher-dimensional physics. Consider a family of 1D systems parameterized by a momentum in a synthetic orthogonal dimension. This momentum is the pump parameter that maps the 1D pump to the 2D quantum Hall system with a first Chern number[6,8]. The topological bulk response of the 1D pump matches that of the 2D quantum Hall effect: varying the pump parameter generates an electromotive force that pushes an integer number of charges per pump cycle across the physical dimension[5]. 1D pumps have recently been demonstrated in cold atom[16,17] and photonic[6,8] experiments.

A 2D topological pump can be subject to two pump parameters, corresponding to a 4D quantum Hall system[7]. In its simplest form, a 4D quantum Hall system is the sum of two 2D quantum Hall systems in disjoint planes[7,27,28], residing in the direct product space associated with the individual models. Correspondingly, a 2D topological pump manifests as the sum of two 1D pumps on orthogonal axes[7]. Here we consider 'off-diagonal' pumps in which the hopping is modulated as a function of the pump parameters[6,8]; that is, we study a 2D tight-binding model of particles that hop on a lattice described by the Hamiltonian (Fig. 1a)

$$H=\sum_{x,y} t_x(\phi_x)c^{\dagger}_{x,y}c_{x+1,y}+t_y(\phi_y)c^{\dagger}_{x,y}c_{x,y+1}+\text{h.c.} \qquad (1)$$

where $c_{x,y}$ annihilates a particle at site (x, y); $t_i(\phi_i)=\tilde{t}_i+\lambda_i\cos(2\pi b_i i+\phi_i)$, with $i\in\{x, y\}$, are modulated hopping amplitudes in the i direction, with bare hopping $\tilde{t}_i$ and modulation λ_i amplitudes. The modulation frequencies b_i are mapped in four dimensions to two magnetic fields in the x–v and y–w planes[7]. The pump parameters ϕ_x and ϕ_y correspond to momenta in the v and w directions, respectively; that is, their modulation dynamically generates electric-field perturbations in these directions. Considering that the pump parameters correspond to additional synthetic dimensions, we characterize bandgaps of the 2D pump with non-trivial second Chern numbers that manifest as a quantized bulk response with 4D symmetry[7].

We realize such a 2D topological pump using arrays of coupled waveguides (Fig. 1b). Each array is constructed to emulate the 2D pump

[1]Institute for Theoretical Physics, ETH Zurich, 8093 Zürich, Switzerland. [2]Department of Electrical and Computer Engineering, University of Pittsburgh, Pittsburgh, Pennsylvania 15261, USA. [3]Department of Physics, The Pennsylvania State University, University Park, Pennsylvania 16802, USA. [4]Department of Physics, Holon Institute of Technology, Holon 5810201, Israel. ‡Deceased.

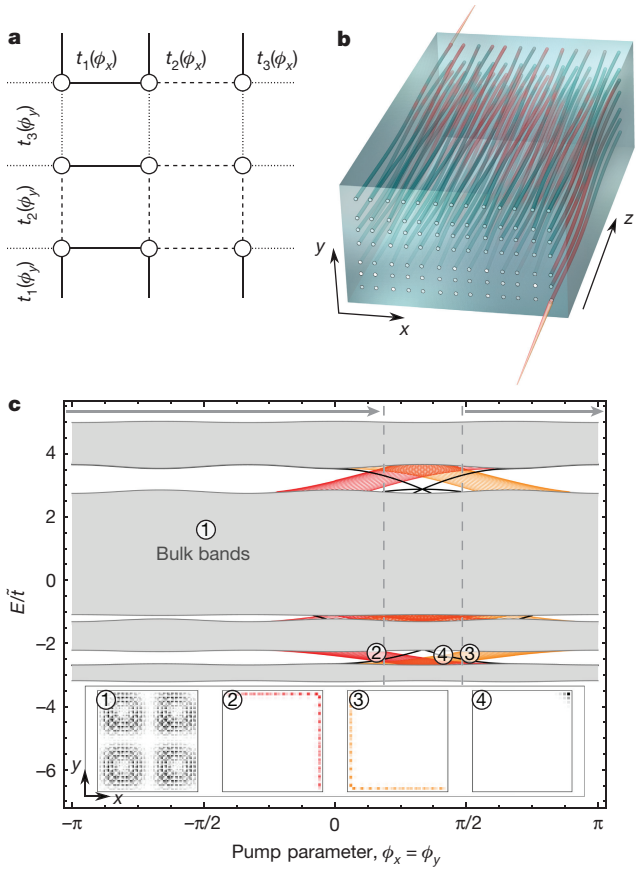

Figure 1 | 2D topological pump and its band structure. a, Schematic of the lattice model (equation (1)) with a 3×3 unit cell, that is, $b_x = 1/3$ and $b_y = 1/3$, resulting in three different hopping amplitudes (solid, dashed and dotted lines) in each direction, which can be modulated using the pump parameters ϕ_x and ϕ_y. **b**, Illustration of the 2D (7×13) array of waveguides with z-dependent spacing. Light is injected into the input facet, is pumped across the array during its propagation (owing to the topological nature of the 2D pump) and is collected on the other side using an InGaAs CCD camera. **c**, Calculated band structure for a similar device, consisting of a 70×70 array of coupled waveguides, where energy E is plotted along the path $\phi_x = \phi_y$ (larger dimensions chosen for clarity) at a wavelength of 1,550 nm, normalized by the bare hopping amplitude $\tilde{t}$. Bulk modes are shown in grey, edge modes in red and orange, and corner modes in black. The insets show representative wavefunctions for each type of mode. For our choice of pump parameters, the edge modes (red and orange) form wedges owing to their degeneracy. The corner modes vanish into the bulk bands along their pump path and weakly hybridize with bulk modes. We perform pumping experiments to study the properties of these boundary states, in which ϕ_x and ϕ_y are scanned between 0.477π and 2.19π (vertical dashed lines; arrows indicate the pumping direction); see Figs 2 and 3.

(equation (1) with $b_x = 1/3$ and $b_y = 1/3$), using 7 rows and 13 columns. The inter-waveguide separation is such that the evanescent coupling between nearest-neighbour waveguides is modulated according to equation (1), with $\lambda_x = \lambda_y = 1.06\,\mathrm{cm}^{-1}$ and $\tilde{t}_x = \tilde{t}_y = 1.94\,\mathrm{cm}^{-1}$ (at a wavelength of 1,550 nm). Nevertheless, the evanescent coupling is a function of both separation and wavelength (Methods, Extended Data Fig. 1). Therefore, the resulting structure has coupling between waveguides beyond its nearest neighbours and the emulated model does not decompose into two disjoint 1D pumps. Despite this, the spectrum for the device demonstrates gap-traversing boundary states, with both edge and corner states (Fig. 1c, Methods, Extended Data Fig. 2).

The appearance of such edge phenomena results from the non-trivial 4D topology of the 2D pump. The 4D symmetry of the second Chern number bulk response generates two types of response: density-type and Lorentz-type[27–29]. The edge bands support the former and the corner modes the latter (Methods). For clarity, we explain the appearance of the topological boundary modes by studying the structure of the model described in equation (1). Because this model can be decomposed into decoupled 1D pumps, each having gaps with non-trivial first Chern numbers[5,6,8], we have the following: (a) the spectrum of the 2D pump is a Minkowski sum of the spectra of the two 1D pumps, $E = E_x + E_y$; (b) the states of the model are product states of the two independent models; and (c) the product bands are associated with second Chern numbers that are equal to the product of the individual first Chern numbers[7]. The third result leads to non-trivial bulk phenomena only when gaps remain open in the summed Minkowski spectra. Importantly, the second Chern number and the corresponding 4D symmetry of its associated bulk responses imply that pumping will occur in response to a scan of either or both pump parameters ϕ_i (Methods).

Let us now consider these properties of the model in equation (1) in an open geometry. Because each 1D pump has 1D bulk modes and zero-dimensional (0D) boundary modes, (a) and (b) above imply that the 2D pump states are grouped into three categories: (i) 2D bulk modes composed of products of 1D bulk modes; (ii) edge modes composed of products of 1D bulk modes with a 0D boundary; and (iii) corner modes that are a product of 0D boundaries. The boundary modes (cases (ii) and (iii)) support the quantized second Chern number response (Methods). The 1D edge states of the 2D system are pumped in response to a single pump parameter and map onto 3D hypersurface states in four dimensions. The 0D corner states are pumped in response to one or both pump parameters and map to 2D hypersurface states. These states highlight the hypersurface phenomena that are associated with the second Chern number.

Our device does not decompose perfectly into two 1D pumps, owing to longer-ranged hopping. Nevertheless, the bulk gaps remain open. As a result, the characterization of these gaps by non-trivial second Chern numbers implies that the bulk response must remain unchanged. The appearance of edge states that traverse the gaps as a function of the pump parameters ϕ_i supports this response in a finite-sized system. Here we probe the behaviour of these states experimentally.

The waveguide array (Fig. 1b) is fabricated using femtosecond-laser writing[30,31] in such a way that each single-mode waveguide couples evanescently to its neighbours. When light is injected into the array, it excites eigenmodes according to their spatial overlap with the input beam. The diffraction of light through the array is governed by the paraxial Schrödinger equation, $i\partial_z\psi = H(z)\psi$, in which the time-evolution coordinate t in the usual Schrödinger equation is replaced by the distance of propagation z; ψ represents the tight-binding wavefunction and $H(z)$ is the Hamiltonian. Therefore, the diffraction of light through the array mimics the time evolution of the wavefunction of a quantum particle. Consequently, time-dependent pumping means adiabatically varying ϕ_i along the waveguide axis[6,8]: $\phi_i \rightarrow \phi_i(z)$.

We demonstrate experimentally the appearance of edge modes in the structure and their behaviour under scans of the pump parameters. We start by studying a structure with straight waveguides, which is therefore invariant in z. We inject light into two different waveguides in the array: one along the left edge and one along the bottom edge. The output light is collected after a diffraction length of 15 cm. Light stays confined largely to the injected edge (it mostly excites the topological localized edge bands; Fig. 2a, b). Additionally, it spreads across the whole edge, implying dispersive bands of edge modes (such as the bands that cross the gaps in Fig. 1c), in accordance with the expected density-type response (Methods). The light stays confined to a single edge as a result of the weak coupling between states on adjoining edges; that is, the long-range coupling does not break the orientation that is associated with the two orthogonal 1D topological pumps embedded in the system. Some of the edge states (case (ii) above) that we excite have the same energies as bulk states in the open system geometry (Methods). These long-lived resonances further demonstrate that the

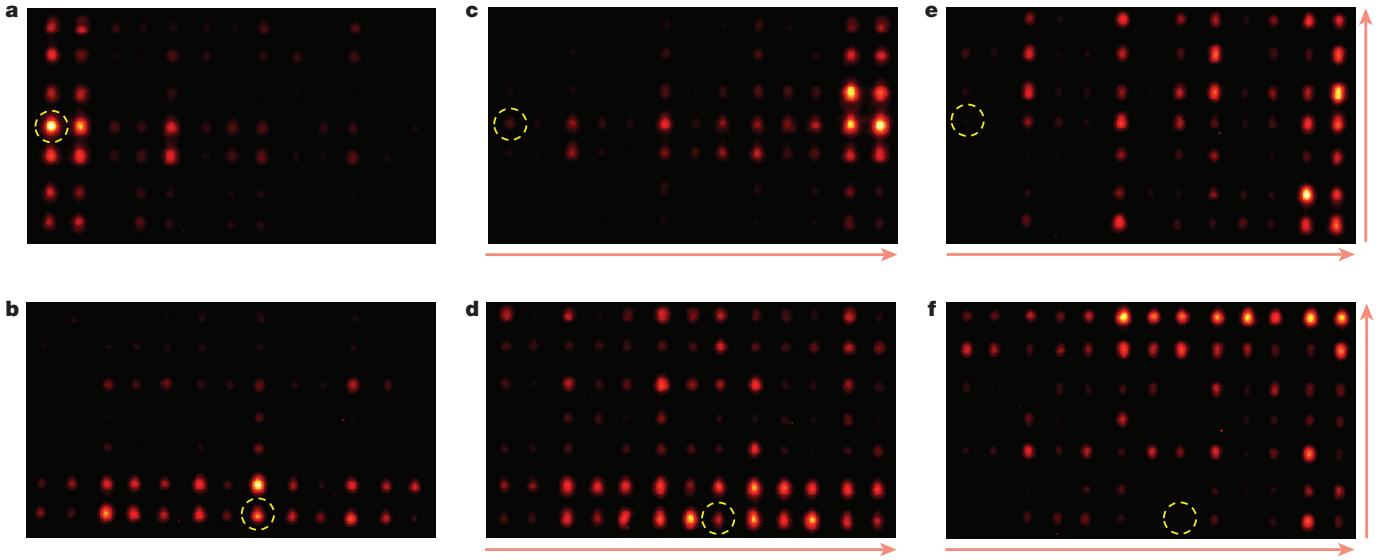

Figure 2 | Edge-to-edge pumping. Images of the output facet of waveguide arrays after $z = 15$ cm of propagation are shown. **a**, **b**, Device with no pumping, corresponding to a model with $\phi_x = \phi_y = 0.477\pi$ (see Fig. 1). Light that is injected at the centre of the left (**a**) or bottom (**b**) edges excites the topological edge bands and spreads out along the edge. **c**, **d**, Pumping of ϕ_x (from 0.477π to 2.19π while ϕ_y is held constant at 0.477π) causes the light injected at the left edge to be pumped to the right (**c**); no such pumping is observed when light is injected at the bottom edge (**d**). **e**, **f**, When ϕ_x and ϕ_y are simultaneously pumped (from 0.477π to 2.19π), light injected at the left (**e**) and bottom (**f**) edges pumps from left to right and bottom to top, respectively. Light in the bulk arises from imperfect coupling to edge states and from deviations from adiabaticity. The yellow dashed circles indicate the injection sites at the input facet ($z = 0$) and the red arrows indicate the direction of pumping. These results demonstrate that edge bands exist in the structure and appear on opposite sides of the device as a function of the pump parameters, in accordance with the density-type bulk response that is implied by the 4D Hall-type band structure of the system.

long-range coupling is a small perturbation of the decoupled model in equation (1).

Having established that we can excite the edge modes of the 2D pump, we demonstrate their behaviour under scans of the pump parameters ϕ_i. We implement edge pumping by allowing the positions of the waveguides to 'wiggle' by varying ϕ_i as a function of z (Fig. 1b). We vary these pump parameters within the range $[0.477\pi, 2.19\pi]$ because localized edge modes exist at these values (a full pumping cycle is not necessary to observe edge pumping from one side of the system to the other). We fabricate separate arrays that correspond to two scenarios: (1) pumping in only the x direction; and (2) pumping in both the x and y directions. In case (1), we see that when light is injected at the left edge, it is pumped to the right edge (Fig. 2c); however, when it is injected at the bottom, it is not pumped to the top because ϕ_y is not pumped (Fig. 2d). In case (2), we observe that the edge states pump both from left to right (Fig. 2e) and bottom to top (Fig. 2f). We injected light with several different input wavefunctions along the edge in question (including single and double waveguide inputs), which resulted in different amounts of overlap of the input wavefunction with each of the edge bands; clear pumping was observed in each case. These results show that an electromotive force applied in the v and w directions induces pumping of edge bands from one 3D (v, w, y) hyperplane to the opposite one in the x direction, and from one 3D (v, w, x) hyperplane to the opposite one in the y direction, as implied by the 4D Hall bulk density-type response (Methods).

We examine the pumping of states at the corners of the arrays for the same range of ϕ_x and ϕ_y as for edge states. The presence of the corner modes (black in Fig. 1c) support the Lorentz-type bulk response (Methods). Depending on the values of ϕ_x and ϕ_y, the corner modes can either be in the bandgap or overlap with bulk modes where they can hybridize to form long-lived resonances. In the experiment, the bottom-left-corner mode is directly excited and pumped along the bottom edge, in conjunction with it being the boundary mode of the 1D pump that crosses edge to edge (Fig. 3a, b). Interestingly, when we scan ϕ_x and ϕ_y simultaneously, the bottom-left-corner mode is pumped mostly to the top-right corner (Fig. 3c) despite any hybridization with bulk modes. Such diagonal pumping under a concurrent ϕ_i scan agrees with the 4D symmetry of the second Chern number bulk response, that is, with the Lorentz-type transverse response (Methods). The photonic diagonal pumping through bulk bands is expected in the decoupled

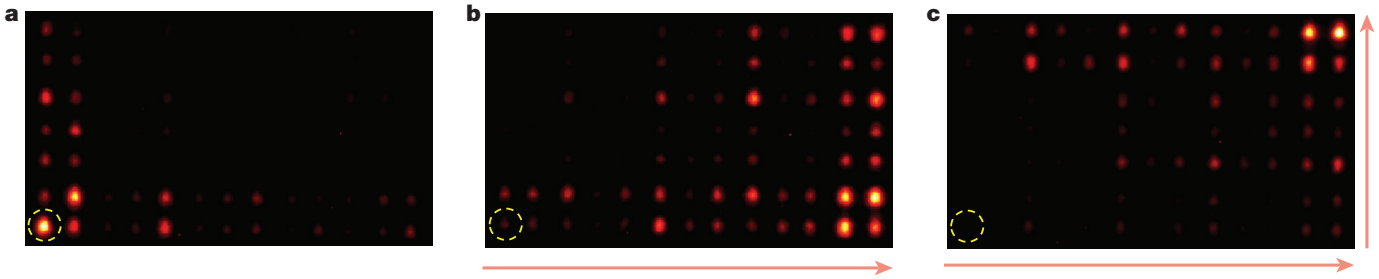

Figure 3 | Corner-to-corner pumping. Images and devices are similar to those described in Fig. 2. **a**, With no pumping, so light stays confined to the corner. **b**, Light is pumped from the bottom-left corner to the bottom-right corner via ϕ_x. **c**, When ϕ_x and ϕ_y are both pumped, the corner state is pumped from bottom-left to top-right. The corner state passes through the bulk band and remains localized because it is a long-lived resonance, not in the bandgap (Methods). Its appearance on the diagonally opposite corner is in accordance with the Lorentz-type response that is implied by the 4D Hall-type band structure of the system.

model (equation (1)), in which each constituent 1D pump is characterized by its own first Chern number and therefore the corner modes manifest as the fully bound joint product of the protected topology at the boundary of the 2D pump. This in turn means that in our set-up the corner modes only weakly hybridize with the bulk and the pumping is carried by long-lived resonances. We note that topological corner modes are unique in the sense that they have two fewer dimensions than the physical dimension of the system (conventional topological modes have one fewer dimension). The appearance and demonstration of such modes has recently been reported in inversion-symmetry-protected 2D systems[32,33].

In conclusion, we have observed topological edge pumping associated with the 4D quantum Hall effect in a 2D photonic system using synthetic dimensions. These observations imply that the system is characterized by a non-zero second Chern number. Boundary phenomena provide an independent observation of the physics implied by the second Chern number of the system, in addition to the measurement of the quantized nonlinear bulk response in a similar model using cold atoms[34]. The realization of 4D quantum Hall physics opens up the possibility of realizing many new physical effects and of answering several open questions, including: whether a bulk measurement of the second Chern number can be realized in photonics via the nonlinear response to synthetic fields; whether arbitrarily high spatial dimensionality can be realized; whether interactions can lead to 4D fractional Hall physics when using synthetic dimensions; and whether there are other physical quantities that are quantized in four dimensions that can be measured directly using synthetic dimensions. Because photonic systems naturally allow for non-Hermitian Hamiltonians (which arise from gain and loss), another question is how non-Hermiticity and topological gaps associated with non-zero second Chern number interact. We expect that experimental access to 4D quantum Hall physics will open up many other directions for research.

Online Content Methods, along with any additional Extended Data display items and Source Data, are available in the online version of the paper; references unique to these sections appear only in the online paper.

Received 23 May; accepted 31 October 2017.

1. Klitzing, K. v., Dorda, G. & Pepper, M. New method for high-accuracy determination of the fine-structure constant based on quantized Hall resistance. *Phys. Rev. Lett.* **45,** 494–497 (1980).
2. Avron, J. E., Sadun, L., Segert, J. & Simon, B. Chern numbers, quaternions, and Berry's phases in Fermi systems. *Commun. Math. Phys.* **124,** 595–627 (1989).
3. Fröhlich, J. & Perdini, B. in *Mathematical Physics 2000* 9–47 (Imperial College Press, 2000).
4. Zhang, S.-C. & Hu, J. A four-dimensional generalization of the quantum Hall effect. *Science* **294,** 823–828 (2001).
5. Thouless, D. J. Quantization of particle transport. *Phys. Rev. B* **27,** 6083–6087 (1983).
6. Kraus, Y. E., Lahini, Y., Ringel, Z., Verbin, M. & Zilberberg, O. Topological states and adiabatic pumping in quasicrystals. *Phys. Rev. Lett.* **109,** 106402 (2012).
7. Kraus, Y. E., Ringel, Z. & Zilberberg, O. Four-dimensional quantum Hall effect in a two-dimensional quasicrystal. *Phys. Rev. Lett.* **111,** 226401 (2013).
8. Verbin, M., Zilberberg, O., Lahini, Y., Kraus, Y. E. & Silberberg, Y. Topological pumping over a photonic Fibonacci quasicrystal. *Phys. Rev. B* **91,** 064201 (2015).
9. Haldane, F. & Raghu, S. Possible realization of directional optical waveguides in photonic crystals with broken time-reversal symmetry. *Phys. Rev. Lett.* **100,** 013904 (2008).
10. Wang, Z., Chong, Y., Joannopoulos, J. & Soljačić, M. Observation of unidirectional backscattering-immune topological electromagnetic states. *Nature* **461,** 772–775 (2009).
11. Rechtsman, M. *et al.* Photonic Floquet topological insulators. *Nature* **496,** 196–200 (2013).
12. Hafezi, M., Mittal, S., Fan, J., Migdall, A. & Taylor, J. Imaging topological edge states in silicon photonics. *Nat. Photon.* **7,** 1001–1005 (2013).
13. Cheng, X. *et al.* Robust reconfigurable electromagnetic pathways within a photonic topological insulator. *Nat. Mater.* **15,** 542–548 (2016).
14. Aidelsburger, M. *et al.* Realization of the Hofstadter Hamiltonian with ultracold atoms in optical lattices. *Phys. Rev. Lett.* **111,** 185301 (2013).
15. Jotzu, G. *et al.* Experimental realization of the topological Haldane model with ultracold fermions. *Nature* **515,** 237–240 (2014).
16. Lohse, M., Schweizer, C., Zilberberg, O., Aidelsburger, M. & Bloch, I. A Thouless quantum pump with ultracold bosonic atoms in an optical superlattice. *Nat. Phys.* **12,** 350–354 (2016).
17. Nakajima, S. *et al.* Topological Thouless pumping of ultracold fermions. *Nat. Phys.* **12,** 296–300 (2016).
18. Slobozhanyuk, A. *et al.* Three-dimensional all-dielectric photonic topological insulator. *Nat. Photon.* **11,** 130–136 (2017).
19. Lu, L. *et al.* Experimental observation of Weyl points. *Science* **349,** 622–624 (2015).
20. Noh, J. *et al.* Experimental observation of optical Weyl points and Fermi arc-like surface states. *Nat. Phys.* **13,** 611–617 (2017).
21. Qi, X.-L., Hughes, T. L. & Zhang, S.-C. Topological field theory of time-reversal invariant insulators. *Phys. Rev. B* **78,** 195424 (2008).
22. Sugawa, S., Salces-Carcoba, F., Perry, A. R., Yue, Y. & Spielman, I. B. Observation of a non-Abelian Yang monopole: from new Chern numbers to a topological transition. Preprint at https://arxiv.org/abs/1610.06228 (2016).
23. Lu, L. & Wang, Z. Topological one-way fiber of second Chern number. Preprint at https://arxiv.org/abs/1611.01998 (2016).
24. Prodan, E., Leung, B. & Bellissard, J. The noncommutative *n*th-Chern number ($n \geq 1$). *J. Phys. A* **46,** 485202 (2013).
25. Boada, O., Celi, A., Latorre, J. & Lewenstein, M. Quantum simulation of an extra dimension. *Phys. Rev. Lett.* **108,** 133001 (2012).
26. Jukić, D. & Buljan, H. Four-dimensional photonic lattices and discrete tesseract solitons. *Phys. Rev. A* **87,** 013814 (2013).
27. Price, H. M., Zilberberg, O., Ozawa, T., Carusotto, I. & Goldman, N. Four-dimensional quantum Hall effect with ultracold atoms. *Phys. Rev. Lett.* **115,** 195303 (2015).
28. Ozawa, T., Price, H. M., Goldman, N., Zilberberg, O. & Carusotto, I. Synthetic dimensions in integrated photonics: from optical isolation to four-dimensional quantum Hall physics. *Phys. Rev. A* **93,** 043827 (2016).
29. Price, H., Zilberberg, O., Ozawa, T., Carusotto, I. & Goldman, N. Measurement of Chern numbers through center-of-mass responses. *Phys. Rev. B* **93,** 245113 (2016).
30. Szameit, A. & Nolte, S. Discrete optics in femtosecond-laser-written photonic structures. *J. Phys. At. Mol. Opt. Phys.* **43,** 163001 (2010).
31. Szameit, A. *et al.* Control of directional evanescent coupling in fs laser written waveguides. *Opt. Express* **15,** 1579–1587 (2007).
32. Benalcazar, W. A., Bernevig, B. A. & Hughes, T. L. Quantized electric multipole insulators. *Science* **357,** 61–66 (2017).
33. Noh, J. *et al.* Topological protection of photonic mid-gap cavity modes. Preprint at https://arxiv.org/abs/1611.02373 (2016).
34. Lohse, M., Schweizer, C., Price, H. M., Zilberberg, O. & Bloch, I. Exploring 4D quantum Hall physics with a 2D topological charge pump. *Nature* **553,** https://doi.org/10.1038/nature25000 (2018).

Acknowledgements We thank H. M. Price, M. Lohse, C.-X. Liu, W. Benalcazar, E. Prodan and T. Ozawa for their comments and feedback on the manuscript. O.Z. thanks the Swiss National Science Foundation for financial support. M.C.R. acknowledges the National Science Foundation under award number ECCS-1509546, the Charles E. Kaufman Foundation, a supporting organization of the Pittsburgh Foundation, and the Alfred P. Sloan Foundation under fellowship number FG-2016-6418. K.P.C. acknowledges the National Science Foundation under award numbers ECCS-1509199 and DMS-1620218.

Author Contributions O.Z., J.G., Y.E.K. and M.C.R. performed the theoretical analysis; S.H. developed the laser fabrication process and characterized the samples with the assistance of J.G. and M.W., under the supervision of K.P.C. and M.C.R.; O.Z. and M.C.R. designed the experiment, wrote the manuscript and supervised the project.

Author Information Reprints and permissions information is available at www.nature.com/reprints. The authors declare no competing financial interests. Readers are welcome to comment on the online version of the paper. Publisher's note: Springer Nature remains neutral with regard to jurisdictional claims in published maps and institutional affiliations. Correspondence and requests for materials should be addressed to O.Z. (zilberberg@itp.phys.ethz.ch) and M.C.R. (mcrworld@psu.edu).

METHODS

Experimental specifications. The experiments were conducted using arrays of evanescently coupled waveguides fabricated in borosilicate glass using femtosecond-laser-writing technology[30,31]. The waveguides are all identical in refractive index and dimension, but the inter-waveguide separation was modulated to realize the off-diagonal 2D model (equation (1)). In all cases, we observe the output image (after 15 cm of propagation) over a range of wavelengths (1,510–1,590 nm) in increments of 5 nm, and then average the output intensities over all wavelengths (Figs 2, 3). We note that the bandgap remains open over this range. We perform the averaging over wavelength to minimize sensitive interference effects due to fabrication imperfections.

Model implementation with waveguide arrays. The diffraction of paraxial light through the structures is governed by the paraxial Schrödinger equation[30,35]:

$$i\partial_z\psi = -\frac{1}{2k_0}\nabla^2\psi - \frac{k_0\Delta n}{n_0}\psi$$

where the wavefunction $\psi(x, y, z)$ corresponds to the electric-field envelope, $\boldsymbol{E}(x, y, z) = \psi(x, y, z)\exp(ik_0z - i\omega t)\hat{\boldsymbol{E}}_0$, $\nabla^2 = \partial_x^2 + \partial_y^2$ is the transverse Laplacian, $\Delta n(x, y, z)$ is the change in refractive index relative to the background index n_0, and $k_0 = 2\pi n_0/\lambda$ is the wavenumber in the background medium. For an array of single-mode, weakly coupled waveguides, the evolution generated by the paraxial Schrödinger equation can be described using tight-binding theory, whereby light hops between the bound modes of adjacent waveguides. The hopping amplitude t associated with a given waveguide separation can be obtained by numerically computing the two lowest eigenvalues E_1 and E_2 of the full equation for a system consisting of two waveguides; the hopping amplitude is then $t = (E_1 - E_2)/2$.

To perform this computation for our waveguides, we used a best-fitting Gaussian model for the variation in the waveguide refractive index: $\Delta n(x, y) = \delta n\exp\left(-x^2/\sigma_x^2 - y^2/\sigma_y^2\right)$, with $\delta n = 2.8\times10^{-3}$, $\sigma_x = 3.50$ μm and $\sigma_y = 5.35$ μm. These parameters were obtained by calibrating over a set of 1D test arrays. Using this profile and a background index of $n_0 = 1.473$, we obtain a model of the form $t(s) = A\exp(-\gamma s)$ for the dependence of the hopping amplitudes on the waveguide separation s. Here $A = A(\lambda)$ and $\gamma = \gamma(\lambda)$ are wavelength-dependent parameters plotted in Extended Data Fig. 1. We obtain these parameters by computing the couplings along the x and y directions separately for different values of s (15–35 μm) at wavelengths of 1,450–1,650 nm and then fitting the average of the x and y couplings to a model of the form given above for the hopping amplitudes. We then used this model to solve for the waveguide spacings that are required to implement the modulated hopping amplitudes defined by the Hamiltonian in equation (1).

To provide a clearer picture of the waveguide configurations used in our photonic system, we include an illustration of a 1D pump in Extended Data Fig. 1b. Varying the waveguide spacings along the propagation direction allows us to control the hopping amplitudes in a way that implements a sweep of the pump parameter ϕ_x. To obtain the full 2D array, we consider additional copies of such a structure stacked vertically along the y direction, with the vertical spacings determined by the hopping amplitudes associated with the y direction.

The decoupled model. Here we examine how the bulk response in an analogous electronic system (that is, one in which states are filled up to a given Fermi level) explains the behaviour of the boundary states. The model in equation (1) decomposes along the x and y directions into a sum of two independent off-diagonal Harper models, $H_x(\phi_x)$ and $H_y(\phi_y)$ (compare with equation (1))[6–8,36]

$$H(\phi_x, \phi_y) = H_x(\phi_x) + H_y(\phi_y) \tag{2}$$

Each $H_i(\phi_i)$ is a one-parameter family of 1D Hamiltonians, that is, a 1D topological pump. Treating the parameter ϕ_i as a Bloch momentum associated with an additional spatial dimension $\tilde{i} \in \{v, w\}$, we perform a dimensional extension of this model and obtain a model that describes the 4D integer quantum Hall system on a lattice with nearest-neighbour hopping in the i direction and next-nearest-neighbour hopping in the $\tilde{i}$ direction[37,38].

For $b = 1/3$, the spectrum of the 1D pump (2D quantum Hall) system consists of three bands (Extended Data Fig. 2a). Each band n has an associated non-zero first Chern number (denoted ν_1 in ref. 34) of

$$\nu_n = \frac{1}{2\pi i}\int_0^{2\pi} C_n(\phi_i, k_i)\mathrm{d}\phi_i\mathrm{d}k_i$$

which is an integral over the Berry curvature (also known as the Chern density) of the filled nth band

$$C_n(\phi_i, k_i) = \mathrm{tr}\left\{P_n\left[\frac{\partial P_n}{\partial\phi_i}, \frac{\partial P_n}{\partial k_i}\right]\right\}$$

where we have defined the spectral projector P_n onto all states in the nth band. Energy gaps in the 2D Hall effect are also characterized by first Chern numbers. The first Chern number of a spectral gap is the sum of first Chern numbers of the bands below that gap in energy. The first Chern number of the bandgap manifests through the quantization of the Hall conductance in response to an applied in-plane electric field; for example, in our case $I_x = (e^2/h)E_v\sum_n\nu_n$, where I_x denotes the current density along the x direction, E_v is an electric field along the v direction, and the sum is over all filled bands. This quantized bulk response has corresponding edge states; that is, gapless boundary states appear in a finite sample (as many as the sum of the Chern numbers of bands below a given gap) and carry the transverse quantized conductance[39].

As discussed in the main text, the eigenstates of the full Hamiltonian (equations (1) and (2)) are tensor products of the eigenstates of the two independent Harper models $|\psi_{mn}\rangle = |\psi_m\rangle\otimes|\psi_n\rangle$, where m enumerates the states in the x–v plane and n those in the y–w plane. Their associated energies are $E_{mn} = E_m + E_n$, so that each pair of bands from the decoupled models yields a band of the 2D pump (4D quantum Hall) model. Therefore, in a finite system, because each constituent 1D pump has bulk and boundary modes, the tensor product eigenstates can be categorized as bulk–bulk, bulk–boundary and boundary–boundary. A colour-coded illustration of the resulting band structure is shown in Extended Data Fig. 2b.

The resulting Minkowski sum spectrum is not always gapped: depending on the amplitudes $\tilde{t}_i$ and λ_i, the joint spectrum may not be gapped. Consequently, if the gaps are closed, then we can no longer discuss the topology of the combined spectrum because any small perturbation will mix the states from the different bands. When the spectral gaps are open, the bulk–boundary and boundary–boundary modes lie for some ϕ_i at energies within the gaps and for others at energies in the bulk bands. Therefore, the boundary–boundary (2D corner) modes that overlap with the bulk are generally expected to become finite-lifetime resonances upon the introduction of higher-neighbour hoppings that destroy the tensor product structure of the eigenstates. Nonetheless, the in-gap bulk–boundary and boundary–boundary modes are protected for arbitrary perturbations that do not close the gap and are the surface states associated with a non-zero second Chern number.

Second Chern number. Let us consider an energy E_j in the jth gap of the 2D pump (4D quantum Hall) system (Extended Data Fig. 2b). The second Chern number (denoted ν_2 in ref. 34) associated with this gap is

$$\mathcal{V}_j = -\frac{1}{8\pi^2}\int\varepsilon_{\mu\nu\rho\sigma}\mathrm{tr}\left\{P_j\frac{\partial P_j}{\partial k_\mu}\frac{\partial P_j}{\partial k_\nu}P_j\frac{\partial P_j}{\partial k_\rho}\frac{\partial P_j}{\partial k_\sigma}\right\}\mathrm{d}^4\boldsymbol{k}$$

where $P_j(\boldsymbol{k})$ is the projector onto the subspace spanned by the eigenstates at Bloch momentum $\boldsymbol{k} = (\phi_x, \phi_y, k_x, k_y)$ with energies below the gap. The subscripts of $\boldsymbol{k}$ mark the vector component. Using the decomposition of H discussed above, $\mathcal{V}_j$ can be written in terms of the first Chern numbers ν_n of the Harper models as[7]

$$\mathcal{V}_j = \sum_{\text{band pairs } m,n \text{ with } E_{mn}<E_j}\nu_n^{xv}\nu_m^{yw}$$

where ν_n^{xv} and ν_m^{yw} are the first Chern numbers associated with the nth band in the x–v plane and mth band in the y–w plane, respectively. Combining this result with the first Chern numbers shown in Extended Data Fig. 2a, the second Chern numbers associated with the lower and upper gaps of the 2D pump (4D quantum Hall) Hamiltonian are $\mathcal{V} = +1$ and -1, respectively. Although the Hamiltonian that governs our photonic system does not decompose in the way discussed above, owing to the presence of higher-neighbour couplings, the upper and lower gaps remain open (see Fig. 1) and, as a result, the associated second Chern numbers remain unchanged.

Bulk responses and their corresponding edge phenomena. Measuring the second Chern number via the bulk response directly requires both an external electric and magnetic field to be applied. However, the presence of the second Chern number implies the presence of surface states, irrespective of the application of external fields. In this section, we explain the relationship between the presence of the surface states in the model and the second Chern number, from the point of view of topological pumping.

The second Chern number of the jth bandgap has an associated quantized nonlinear bulk response

$$I_\alpha = \frac{\mathcal{V}_j}{2}\frac{e^2}{h\Phi_0}\varepsilon_{\alpha\beta\gamma\delta}B_{\beta\gamma}E_\delta$$

where I_α denotes the current density along the α direction, Φ_0 is the flux quantum, E_δ is an electric-field perturbation along the δ direction, $B_{\beta\gamma}$ is a magnetic-field perturbation in the β–γ plane, and $\varepsilon_{\alpha\beta\gamma\delta}$ is a Levi–Civita symbol that highlights

the 4D non-commutative nature of the response. The second Chern number $\mathcal{V}_j$ is defined as the sum over all bands up to the jth of a 4D volume integral over a generalized 4D Berry curvature of the given band.

In our spinless case, we can write the 4D Berry curvature in terms of the 2D Berry curvatures that exist in the two orthogonal planes associated with the independent models[6,8,27–29]. Let us consider these orthogonal planes to be x–v and y–w. In addition, for the choice of boundary conditions in our experiment, let us focus on the responses in the direction $\alpha = x$ and study their bulk–edge correspondence. The responses in the $\alpha = y$ direction will be similar. Having fixed the response direction, there are various choices for the orientation of the perturbing fields in four dimensions. These can be split into density-type responses and Lorentz-type responses.

Density-type response. Consider the case where the extrinsic perturbing field $B_{\beta\gamma}$ is set in a plane for which there is a non-trivial Berry curvature from the underlying model. For responses in the $\alpha = x$ direction, this occurs when $\beta\gamma = yw$. Correspondingly, the orientation of the electric-field perturbation is $\delta = v$. Owing to the non-trivial intrinsic Berry curvature in the x–v plane, E_v also generates a 2D quantum Hall-like response, and the bulk response is

$$I_v = I_y = I_w = 0$$
$$I_x = \frac{e^2}{h}\nu^{xv}\tilde{n}E_v + \frac{e^2}{h\Phi_0}\mathcal{V}_j E_v B_{yw}$$

where ν^{xv} contains the sum over first Chern numbers of filled bands. It is now apparent why we denote this response as 'density-like'. The bulk response has a 2D quantum Hall-like response, multiplied by a particle-density factor $\tilde{n}$ that results from the integration over the 4D volume. The second Chern number response here can be understood[40] to be a Streda formula correction to $\tilde{n}$.

To support such a response in finite-sized systems, the corresponding edge phenomena must manifest a band of modes that traverse the gap. The density of this edge band is modulated by the magnetic-field perturbation. In addition, from the response to E_v we conclude that the in-gap band is dispersive with respect to k_v. Repeating this argument for the density-type response in the y direction, we expect an additional in-gap band that is dispersive with respect to k_w.

In 2D topological pumping, we generate the electric field E_v using Faraday's law of induction, that is, by modulating ϕ_x. Correspondingly, the density-type quantized 4D quantum Hall response implies that within a full 0–2π cycle of ϕ_x a band of states (corresponding to $\tilde{n}$) must cross the gap and appear ν^{xv} times on either side of the x-direction open boundary conditions. The density of this band is modulated by the external magnetic-field perturbation and thus accommodates the density-type second Chern number response. Following the same arguments, similar bands must appear upon scans of ϕ_y to support the response in the $\alpha = y$ direction. In the photonic experiment, we excite these edge bands directly (as well as, inevitably, in-bulk bands) and show that they truly carry modes from one side of the sample to the other in both the x and y directions.

From the above discussion, it is apparent that the observation of edge-to-edge pumping implies that a full band spectrum supports density-type second Chern bulk responses, and it suffices to see these responses as a function of scans of ϕ_x and ϕ_y. In terms of edge physics, adding a perturbing B_{yw} field is not illustrative: the intrinsic field has already set up the conditions (via the density response) for a current that arises from both the first and second Chern numbers.

Lorentz-type responses. Consider the case where the extrinsic perturbing field $B_{\beta\gamma}$ is set in a plane for which there is no Berry curvature from the underlying model. For responses in the $\alpha = x$ direction, this occurs when $\beta\gamma \in \{vy, vw\}$. Correspondingly, the orientation of the electric-field perturbation is $\delta \in \{w, y\}$. We are interested in 2D topological pumping, that is, in generating the electric field using Faraday's law of induction; consequently, we do not apply the electric-field perturbation in the y direction. Because we cannot apply a B_{vw} perturbation between the two dynamical axes of the pump, we are left with the response

$$I_x = \mathcal{V}_j \frac{e^2}{h\Phi_0}\varepsilon_{xvyw}B_{vy}E_w$$

Because E_w is generated by pumping ϕ_y, this response means that $\mathcal{V}_j$ charge-carrier modes must appear within the gap every $1/B_{vy}$ cycles on each side of the x axis.

In the 2D model, the Lorentz-type magnetic-field perturbation enters (in the correct gauge) as a spatial modulation of the model, by changing the modulated hopping:

$$t_x(\phi_x) \to \tilde{t}_x + \lambda_x\cos(2\pi b_x x + 2\pi B_{vy}y + \phi_x)$$
$$t_y(\phi_y) \to \tilde{t}_y + \lambda_y\cos(2\pi b_y y + \phi_y)$$

In the y–w plane, a first Chern number bulk response occurs as a function of scans of ϕ_y, leading to a gradual change in the coordinate y. Therefore, owing to the magnetic-field perturbation B_{vy}, as ϕ_y is scanned a slow modulation of the potential in the x direction also occurs.

This is a slow modulation that would mean that $1/B_{vy}$ cycles of ϕ_y generate in the same time a full scan of ϕ_x from 0 to 2π (see also the bulk-pumping experiment in cold atoms[34]). In a finite-sized system, this Lorentz-type bulk response implies that boundary modes must appear and cross the gap in response to a joint modulation of both pump parameters ϕ_x and ϕ_y: this is precisely the corner mode shown in black in Fig. 1c and Extended Data Fig. 2b, and for these gaps $|\mathcal{V}_j| = 1$.

Data availability. The data that support the findings of this study are available from the corresponding authors on reasonable request.

35. Fleischer, J. W., Segev, M., Efremidis, N. K. & Christodoulides, D. N. Observation of two-dimensional discrete solitons in optically induced nonlinear photonic lattices. *Nature* **422,** 147–150 (2003).
36. Harper, P. G. Single band motion of conduction electrons in a uniform magnetic field. *Proc. Phys. Soc. A* **68,** 874–878 (1955).
37. Kraus, Y. E. & Zilberberg, O. Topological equivalence between the Fibonacci quasicrystal and the Harper model. *Phys. Rev. Lett.* **109,** 116404 (2012).
38. Hofstadter, D. R. Energy levels and wave functions of Bloch electrons in rational and irrational magnetic fields. *Phys. Rev. B* **14,** 2239–2249 (1976).
39. Hatsugai, Y. Chern number and edge states in the integer quantum Hall effect. *Phys. Rev. Lett.* **71,** 3697–3700 (1993).
40. Středa, P. Theory of quantised Hall conductivity in two dimensions. *J. Phys. Chem*. **15,** L717–L721 (1982).

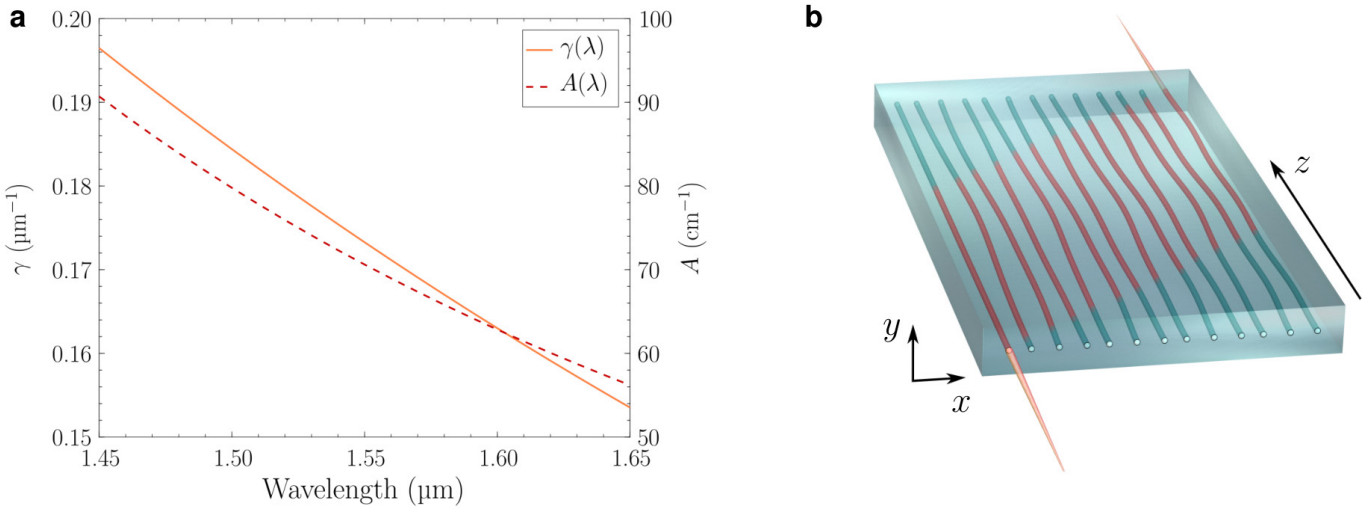

Extended Data Figure 1 | Waveguide coupling parameters and illustration of a 1D pump. a, The overall scale A (dashed red line) and exponential decay prefactor γ (solid orange line) that describe the inter-waveguide coupling as a function of their separation s: $t(s) = A\exp(-\gamma s)$. The parameters were obtained using a thorough calibration procedure (see Methods) and are plotted as a function of wavelength. **b**, An additional illustration of the waveguide spacing used to implement our topological pump. To simplify the diagram, we show a 1D waveguide array, which corresponds to an implementation of a 1D pump. This configuration can be thought of as resulting from a constant y slice through the full 2D waveguide array.

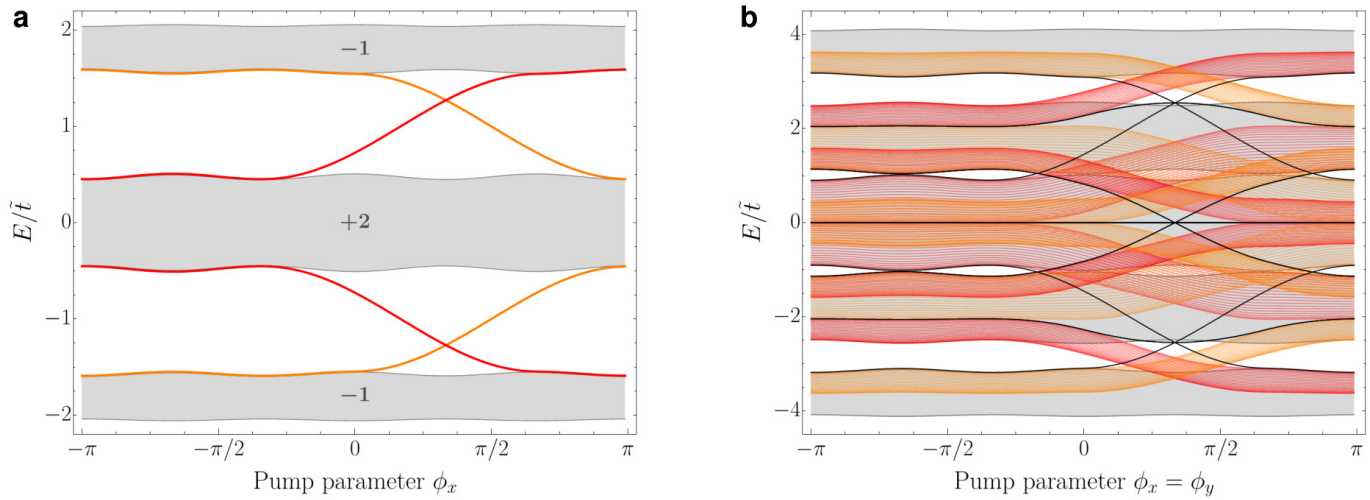

Extended Data Figure 2 | Nearest-neighbour band structure obtained from two decoupled models. See equation (2). **a**, Finite-sample band structure (energy E versus pump parameter) for a single Harper model aligned along the x direction. Boundary modes highlighted in orange (red) are localized on the left (right) end of the 1D sample. The first Chern number associated with each bulk band is also shown. **b**, Band structure for the fully separable 2D pump taken along the path $\phi_x = \phi_y$ for a system that decomposes into two independent Harper models. Each band in **b** is obtained by summing a pair of bands from **a**. The resulting bands can be classified by the types of state that appear in the sum: bulk–bulk (2D bulk), bulk–boundary (2D edge) or boundary–boundary (2D corner). These types are respectively coloured grey, red or orange, and black. As a function of ϕ_i, the edge modes form 'dispersive' bands that thread through the 2D bulk gaps. The corner modes thread between the edge bands and are therefore forced to cross 2D bulk bands along their ϕ_i trajectory.